

SYNCHRONIZATION AND DETECTION FOR TRANSMITTED REFERENCE UWB SYSTEMS

Relja Djapic, Geert Leus and Alle-Jan van der Veen

In this paper we present a synchronization scheme for multiuser transmit-reference ultrawide band (TR-UWB) systems. The proposed blind deterministic synchronization algorithm delivers a fine resolution data packet offset estimate by processing blocks of the received data sequence. The complexity of the algorithm is considerably reduced by exploiting the property that a time domain shift corresponds to a phase rotation in frequency domain. In the simulations the whole transceiver chain is considered taking into account measured channel impulse responses in a typical university building.

1. Introduction

Impulse radio (IR) or ultrawide band (UWB) is a carrierless system which conveys the information by extremely short pulses (inferior to a ns). Such a system possesses a large bandwidth and accordingly a possibility to accommodate high data rate communications. In addition, such a bandwidth introduces a large number of signal processing issues [1].

Deployment of narrow pulses, also known as *monocycles*, results in a high resolution channel impulse response (CIR) that can be several orders of magnitude longer than the pulse itself [2]. Resolving differences in path delays of 1ns becomes possible, as the resolution of the channel is proportional to the width of the transmitted pulse.

The high resolution CIR make the processing schemes deployed in carrier based systems quite unpractical. For instance, sampling at Nyquist rate (order of $\sim 10\text{GHz}$) and use of a RAKE receiver would lead to a huge computational complexity and are unsuitable for the targeted low power, low cost UWB transceiver devices.

A transmitted reference ultrawide band (TR-UWB) scheme, introduced by Hoctor and Tomlinson [3] avoids the channel estimation step. In such a transceiver scheme, pulses are always transmitted in pairs (*doublets*). They both propagate through the same multipath channel. At the receiver, the reference pulse is used as a template in the detection of the second, data modulated pulse.

Two modulation schemes are applicable in a TR-UWB scheme. Using pulse position modulation (PPM) the location of the second pulse with respect to the reference pulse is varied in accordance with the data sequence. On the other hand, pulse amplitude modulation (PAM) is applicable, in which the information pulse can take values from $\{+1, -1\}$.

A receiver used in a TR-UWB system comprises an analog and a digital part. The received sequence is first delayed

and correlated (multiplied) with its non-delayed version. By subsequent integration, the energy that is spread out by the channel is collected. At this point sampling is performed, now at a rate of $\sim 100\text{MHz}$. With the proposed receiver design, a part of the complexity is transferred from the digital to the analog domain making the scheme realistic to implement by the current state of technology.

A detailed data model for a single user TR-UWB scheme is derived in [4] assuming perfect synchronization at the receiver side. This work has been extended to the asynchronous single and multiple user case case in [5] and [6], respectively. Note that the data models in [5,6] are based on the expected signal appearance at the output of the analog part of the receiver. In that manner, long lasting simulations that would involve long, high resolution CIRs are avoided.

In this paper we present a blind, deterministic, high resolution synchronization scheme for multiuser TR-UWB systems. The algorithm estimates the offset of the user of interest by processing the blocks of received data stacked in a matrix such that a shifted version of the user specific code appears in its column span. The property that a time shift corresponds to a phase rotation in the frequency domain and the use of a fast Fourier transformation reduces significantly the complexity of the proposed scheme. In contrast to, [5,6] the algorithm is now verified following the complete transceiver chain and using measured channel impulse responses.

2. Data Model

In this work we consider a transmit-reference ultrawide band (TR-UWB) system. The structure of the transmitted pulse stream is presented by solid lines on the top part of figure 1. A doublet comprises a reference and an information pulse, $g(t)$ and $g(t - D_i)$, respectively. Here, D_i , with $i = 1, 2, \dots, M$, represents the mutual separation of the two pulses within a doublet and is in accordance with a user specific time-hopping (TH) code [7]. A doublet lays within a time interval called a *frame*. The duration of a frame, T_d , is selected to be $T_d > T_h + 2 \max D_i$ in order to avoid inter frame interference (IFI). Every frame is generally repeated N_d times to form a *chip* of duration $T_c = N_d T_d$. A data symbol is of duration $T_s = N_c T_c$, where N_c represents the number of chips. Within the $kN_c + j$ -th chip, the information pulses are modulated by $s_k c_j$, where $s_k \in \{-1, +1\}$ is the k -th data symbol ($k = \dots, -1, 0, 1, \dots$) and $c_j \in \{-1, +1\}$ is the j -th code symbol ($j = 0, 1, \dots, N_c - 1$) of a CDMA kind of code. The overall user's code is a combination of both the TH and CDMA code and is the same for all symbols *i.e.*, a *short code* is used. Let us define a reference pulse for the k -th data symbol, j -th chip, and d -th doublet or frame

¹This research was supported in part by the Dutch Min. Econ. Affairs/Min. Education Freeband-impulse project *Air-Link* and by NWO-STW under the *VICI* programme (DTC.5893).

($d = 0, 1, \dots, N_d - 1$) as

$$g_{k,j,d}(t) = g(t - kT_s - jT_c - dT_d).$$

Without loss of generality, we assume that a reference pulse is placed at the beginning of a frame. Hence, the transmitted sequence, structured as in figure 1, comprising reference and information pulses becomes

$$t_x(t) = \sum_k \sum_{j=0}^{N_c-1} \sum_{d=0}^{N_d-1} \sum_{i=1}^M [g_{k,j,d}(t) + s_k c_j g_{k,j,d}(t - D_i)] J_{i,j},$$

where $J_{i,j}$ determines the time-hopping pattern for each chip, such that $J_{i,j} = 1$ in case delay D_i is utilized in all frames within the j -th chip, and $J_{i,j} = 0$ otherwise. Let $h(t) = h_p(t) * g(t)$ represents the convolution of the transmitted pulse $g(t)$ and the channel impulse response $h_p(t)$, depicted by dashed lines on the top part of figure 1. Using the same index notation for $h(t)$ as for $g(t)$ the received signal in the single user case can be written as

$$r(t) = \sum_k \sum_{j=0}^{N_c-1} \sum_{d=0}^{N_d-1} \sum_{i=1}^M [h_{k,j,d}(t) + s_k c_j h_{k,j,d}(t - D_i)] J_{i,j}.$$

At the receiver side an autocorrelation receiver is deployed [4, 5]. The received signal $r(t)$ is passed through a delay bank with delays D_m , $m = 1, \dots, M$. Every delayed version of the received signal $r(t - D_m)$ is then correlated with $r(t)$ and subsequently integrated with a sliding window integrator of duration $W = T_c$. Note that up to this point all processing is performed in the analog domain facilitating recollection of the transmitted pulse energy spread by a long channel impulse response. In this manner, the need to sample $r(t)$ at the Nyquist rate, which is $\sim 10\text{GHz}$, is avoided. The output of m -th integrator is presented at the bottom of figure 1 and can be described as [4]

$$x_m(t) = \sum_k \sum_{j=0}^{N_c-1} \sum_{i=1}^M p(t - kT_s - jT_c - \tau) [\alpha_{m,i} c_j s_k + \beta_m] J_{i,j}, \quad (1)$$

where, $\alpha_{m,i}$ and β_m represent unknown channel dependent coefficients defined as $\alpha_{mi} = \rho(D_i - D_m) + \rho(D_i + D_m)$ and $\beta_m = 2\rho(D_m)$ where

$$\rho(\Delta) = \int_{-\infty}^{\infty} h(t)h(t - \Delta) dt \quad (2)$$

corresponds to the channel auto-correlation function in the single user case. The scaling $\alpha_{m,i}$ is maximal for matching transmit and receive delays ($D_i = D_m$) [4]. In the case of non-matching delays $D_i \neq D_m$, some residual information remains and we have $\alpha_{m,i} \neq 0$. The coefficient β_m depends only on the receive delay D_m and represents a DC offset. Some typical values of these parameters are presented in [4].

Furthermore, τ depicts an onset of the transmitted data sequence with respect to the beginning of the analysis window at the receiver side. This is an unknown parameter that we tend to estimate in this work. As a short code design is assumed for both the TH and CDMA code ($J_{i,j}$ and c_i), we may constrain τ to the interval $\tau \in [0, T_s)$. A delay corresponding to a multiple of the symbol duration T_s can further be determined by detecting the change in the energy of the received data symbols (transfer from 0 to ± 1 energy level), see data model in figure 3.

The output of the first (second) integrator, $x_1(t)$ ($x_2(t)$), will collect most of the energy from the doublets spaced

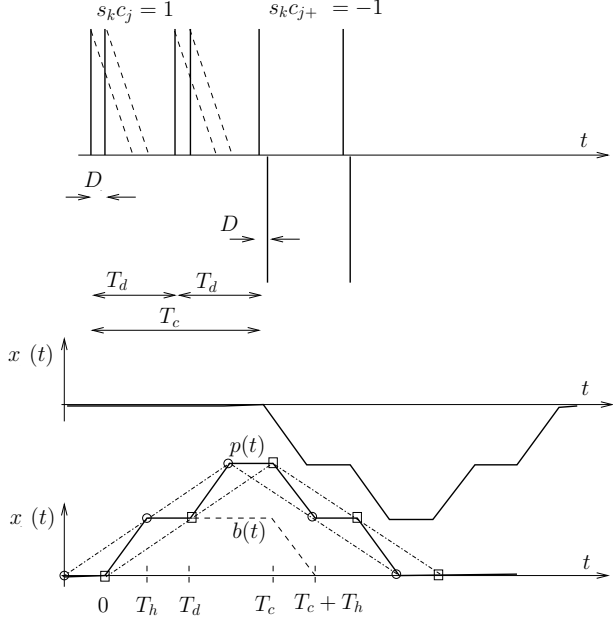


Figure 1. Top:transmitted sequence structure. Bottom: Signal at the output of the analog part of the receiver.

by D_1 (D_2), *i.e.*, for matched transmit and receive delays $D_i = D_m$ (see bottom part of figure 1). To keep the figure simple, we do not plot the signals that arise from non-matching delays $D_i \neq D_m$ nor the effect of the DC offset β_m . After the energy of the channel is collected by means of correlation, a sliding window integration will create a 'tent' pulse shape, $p(t)$. The rising and falling edges of this shape are of duration T_h and equal the length of the composite channel impulse response $h(t)$. They correspond to the regions where the sliding window enters and leaves the regions where the channel energy is present. Each flat part of $p(t)$ portrays the region from a point where the channel is completely faded to the arrival of a new doublet. As a sliding window integrator of duration $W = T_c$ is employed, the 'tent' pulse shape will be smeared over two consecutive chip intervals. Note that the rising and falling edges of $p(t)$ are determined by the duration and the shape of the unknown composite channel impulse response. Nevertheless, in case sampling is performed once per interval T_d , *i.e.*, at frame rate, $p(t)$ can be equivalently represented by a triangular pulse shape, as depicted by the dash-dotted lines in figure 1. Note that the position of the 'triangle' depends on the initial sampling instant, thus a certain ambiguity remains but it is restricted to $[0, T_d)$. Sampling at the beginning and the end of the composite channel produces the samples of an assumed 'triangular' pulse shape represented by the squares and circles in figure 1, respectively. Even if the ambiguity is present, the estimated time offset will collect sufficient signal energy when a decorrelating receiver is employed for symbol estimation.

Using the 'triangular' model for $p(t)$, it is possible to separate the user specific codes from the channel coefficients and data symbols, facilitating the synchronization process.

$$\mathbf{P}_{(N_c+1)P \times N_c} = \begin{bmatrix} \text{triangle} & & & \\ & \text{triangle} & & \\ & & \text{triangle} & \\ & & & \text{triangle} \end{bmatrix}$$

Figure 2. The structure of the \mathbf{P} matrix.

Notice that $x_m(t)$, obtained at the output of the analog receiver part, is of much smaller bandwidth compared to $r(t)$. In this manner, sampling of $x_m(t)$ can be carried out at rates that are realistic for the current state of technology. Hence, at this point, a transition from the analog to the digital domain is performed by sampling $x_m(t)$ at rate P/T_c , where P is chosen equal to N_d , in order to be able to use a 'triangular' shape for $p(t)$, as explained earlier. The sampled version of the sequence at the output of integrator m , *i.e.*, $x_{m,n} = x_m(nT_c/P)$ can now be written as

$$x_{m,n} = \sum_{k=-\infty}^{\infty} \sum_{j=0}^{N_c-1} \sum_{i=1}^M p_{n,j+kN_c} [\alpha_{m,i} c_j s_k + \beta_m] J_{i,j}$$

where $p_{n,j} = p(nT_c/P - jT_c - \tau)$. We then collect $N_c P$ samples in a column vector

$$\mathbf{x}_{m,k} = [x_{m,kN_c P}, \dots, x_{m,(k+1)N_c P-1}]^T,$$

and subsequently collect the outputs of all $m = 1, \dots, M$ integrators in a single matrix

$$\mathbf{X}_k = [\mathbf{x}_{1,k}, \dots, \mathbf{x}_{M,k}].$$

For the asynchronous single user case, where multiple data symbols are encountered, we then obtain the data model depicted in figure 3, as detailed in [5]. Observe that each data symbol s_k is spread over two adjacent received data blocks, \mathbf{X}_k and \mathbf{X}_{k+1} . In order to collect one complete copy of the code in the data model, we therefore collect the received data blocks \mathbf{X}_k in a block Hankel matrix \mathbf{X} . In figure 3, we have used $\mathbf{Z} = \mathbf{P} \text{diag}(\mathbf{c}) \mathbf{J}^T : ((N_c + 1)P \times M)$, which represents the known user specific "code matrix", and $\mathbf{q} = \mathbf{P} \mathbf{J}^T \mathbf{1} : ((N_c + 1)P \times 1)$, which represents a fixed column vector that is related to the bias. Note that $[\mathbf{P}]_{ij} = p((i-1)\frac{T_c}{P} - (j-1)T_c) : ((N_c + 1)P \times N_c)$ contains a sampled version of the triangular pulse shape $p(t)$ per column, as depicted in figure 2, $[\mathbf{J}]_{i,j+1} = J_{ij} : (M \times N_c)$ contains the TH code, and $[\mathbf{c}]_{j+1} = c_j$ contains the CDMA code. $\mathbf{Z}'(\mathbf{q}')$ and $\mathbf{Z}''(\mathbf{q}'')$ represent the 'tail' and the 'head' of $\mathbf{Z}(\mathbf{q})$, respectively. Further, we denote $[\mathbf{A}]_{mi} = \alpha_{mi} : (M \times M)$ and $[\mathbf{b}]_m = \beta_m : (M \times 1)$ as the matrix and vector that collect the channel scaling (α_{mi}) and bias (β_m) coefficients from all integrator outputs, respectively. The current data symbol is multiplied by the complete 'block code' \mathbf{Z} shifted by the unknown offset τ with respect to the beginning of the received data block. By stacking two received blocks one over the other, \mathbf{Z} will be spread over two block intervals. Note that the fact that $\mathbf{Z} = [\mathbf{Z}'^T \ \mathbf{Z}''^T]^T$ can be exploited in the synchronization process to augment the energy of the code we are searching for. The structure presented in figure 3 can compactly be written as

$$\mathbf{X} = \mathbf{G} \mathbf{S} = [\mathbf{G}' \ \mathbf{1}] [\mathbf{S}'^T \ \mathbf{b}'^T]^T, \quad (3)$$

where \mathbf{G} comprises the complete block code and shifts thereof (\mathbf{Z}, \mathbf{Z}' and \mathbf{Z}'') and an all-one column vector, which is due to the fact that \mathbf{q} can be well approximated by an all-one column vector because of the structure of \mathbf{P} and \mathbf{J} . \mathbf{S}' collects the first three block rows of the data matrix \mathbf{S} while \mathbf{b}' represents a stacking of several \mathbf{b} vectors. The data model (3), depicted in figure 3, is taken as the starting point for the multiuser case analysis considered in this paper.

3. Multiuser case

The extension of the single user data model given in (3) to the multiuser case can in general not be achieved by simple linear extension. This is due to the deployment of the autocorrelation receiver. First of all, different users encounter different propagation channels that lead to different auto-correlation functions ρ , as defined in (2). In addition to this, cross-correlation terms arise as a result of the multiplication of channels allocated to different users. After the integration, cross-correlation terms related to user p and user q rely on

$$\rho^{pq}(\Delta) = \int_{-\infty}^{\infty} h^p(t) h^q(t - \Delta) dt.$$

Here, $h^p(t)$ and $h^q(t)$ represent the channel impulse responses of user p and q , respectively. Note that the number of cross-correlation terms increases exponentially with the number of users. Corollary, an increased amount of terms that we consider as interference will appear.

As the channel impulse responses are quite long and mutually uncorrelated we can assume that the cross-correlation terms are small compared to the auto-correlation terms, and we may set $\rho^{pq} = 0$. Under this presumption only auto-correlation terms remain leading to

$$\mathbf{X} = \mathbf{G} \mathbf{S} = [\mathbf{G}'^{(1)} \dots \mathbf{G}'^{(N)} \ \mathbf{1}] [\mathbf{S}'^{(1)T} \dots \mathbf{S}'^{(N)T} \ \mathbf{b}'^T]^T \quad (4)$$

where the superscript (i) , with $i = 1, \dots, N$, represents the user index. Note that all vectors $\mathbf{b}^{(i)}$ merge to a single vector \mathbf{b}' due to the linear dependence of the all-one vectors $\mathbf{1}$.

4. Synchronization

The synchronization scheme for a single user case derived in [5] is now also applicable for the multiuser case. We consider user one to be the user of interest and synchronize to it without loss of generality. Assuming no noise and zero cross-correlation terms, $\mathbf{G}'^{(1)}$ that contains block code $\mathbf{Z}^{(1)}$ and parts thereof ($\mathbf{Z}'^{(1)}$ and $\mathbf{Z}''^{(1)}$) is orthogonal to the left nullspace of \mathbf{X} , *i.e.*,

$$\mathbf{U}_0^H \mathbf{G}'^{(1)} = \mathbf{0} \quad (5)$$

where superscript H represents the complex conjugate transpose. Using a similar transformation as in [5] originating from [8] yields the following expression we need to minimize in order to determine the packet offset τ of the user of interest $i = 1$ (we now assume that noise and cross-correlation terms are present and represent interference terms):

$$\underset{\tau}{\text{argmin}} \|\mathbf{Z}'_{\tau}^{(1)H} \mathcal{U}_0\|^2 = \underset{\tau}{\text{argmin}} \|\mathbf{z}'_{1,\tau}^{(1)H} \mathcal{U}_0\| \dots \|\mathbf{z}'_{M,\tau}^{(1)H} \mathcal{U}_0\|^2 \quad (6)$$

where $\mathbf{Z}'_{\tau}^{(1)}$ corresponds to the mid column of $\mathbf{G}'^{(1)}$ and contains a known code $\mathbf{Z}^{(1)}$ shifted by an unknown τ that takes any value in the range $\tau \in [0, T_s)$. \mathcal{U}_0 is created from

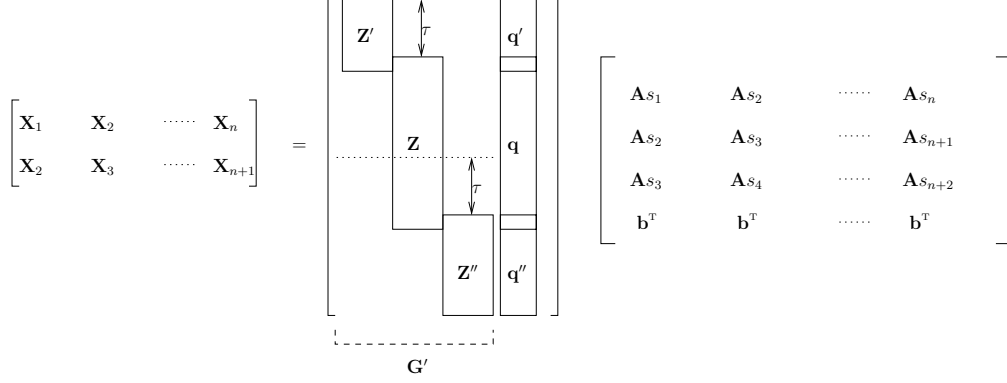


Figure 3. Block data model $\mathbf{X} = \mathbf{G}\mathbf{S}$ for the asynchronous single user case using a TR UWB scheme.

the column vectors of the zero subspace \mathbf{U}_0 . $\mathbf{z}_{i,\tau}^{(1)}$ depicts the i -th column of $\mathbf{Z}_\tau^{(1)}$. Inserting $\mathbf{I} = \mathbf{F}^H \mathbf{F}$ between $\mathbf{z}_{i,\tau}^{(1)H}$ and \mathcal{U}_0 , with \mathbf{F} representing the unitary Fourier transformation matrix, and using the fact that a shift in the time domain corresponds to a phase rotation in the frequency domain, we can rewrite (6) as

$$\begin{aligned} & \operatorname{argmin}_\tau \|\tilde{\mathbf{z}}_1^{(1)H} \mathbf{D}_\tau^* \tilde{\mathcal{U}}_0 \cdots |\tilde{\mathbf{z}}_M^{(1)H} \mathbf{D}_\tau^* \tilde{\mathcal{U}}_0 \|^2 \\ &= \operatorname{argmin}_\tau \|\phi_\tau^H [\operatorname{diag}(\tilde{\mathbf{z}}_1^{(1)H}) \tilde{\mathcal{U}}_0 \cdots |\operatorname{diag}(\tilde{\mathbf{z}}_M^{(1)H}) \tilde{\mathcal{U}}_0 \|^2 \\ &= \operatorname{argmin}_\tau \|\phi_\tau^H \mathcal{K} \|^2, \end{aligned} \quad (7)$$

where $\tilde{\mathbf{z}}_i^{(1)H} = \mathbf{z}_{i,0}^{(1)H} \mathbf{F}^H$ depicts the inverse Fourier transformation of a known non-delayed version of the code vector $\mathbf{z}_{i,0}^{(1)H}$. $\tilde{\mathcal{U}}_0 = \mathbf{F} \mathcal{U}_0$ correspond to the Fourier transformation of \mathcal{U}_0 , while $\phi_\tau = \operatorname{diag}(\mathbf{D}_\tau) = [1, \dots, e^{-j2\pi\tau/(2N)}]^T$. Superscript * specifies the complex conjugation. Due to the structure of ϕ_τ , the integer part of the delay τ , corresponds to the ordinal number of the row with the lowest norm of the matrix $\mathbf{F}^H \mathcal{K}$. An additional MUSIC-like search provides the fractional part of the packet offset estimate.

5. Simulations

In this section the performance of the synchronization algorithm is evaluated using measured channel impulse responses. Note that in our previous work [5, 6], a simplified model was used in the simulations where the received data signal was generated at the output of the integrators rather than at the receive antenna. Assumptions that after integration a triangular pulse shape arises and that the noise at that point is white Gaussian were deployed. In this manner, complex operations such as the convolution with the long channel impulse responses, the correlation operations, and the integration steps have been avoided.

In this work, we test the model introduced in [5, 6] following the complete transceiver chain. The channel impulse responses used in these simulations are obtained by measurements in a typical university building. The following scenarios are taken into account: 1) office, 2) corridor, 3) corridor-to-office, 4) library, and 5) office-to-office. Both line of site and non line of site channel impulse responses are covered in this fashion.

A sampling rate of 10ps is used in the channel measurements. After the receive antenna a bandpass filtering is performed to limit the bandwidth of the observed signal to the interval 3 – 10GHz, as recommended by FCC regu-

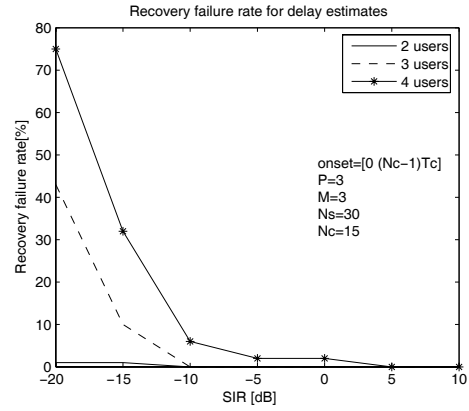


Figure 4. The percentage of incorrectly estimated packet offsets.

lations. The filtering step reduces the impact of the noise and the low frequency interference. We limit the measured channel impulse responses to the interval $[0, 50]$ ns, as the contribution of the channel components that fall outside this interval is insignificant. The duration of the frame is chosen to be $T_d = 60$ ns.

We define the signal to interference ratio (SIR) as $SIR = 10 \log(P_1/P_I)$. P_1 represents the energy of a single data symbol of the user of interest $i = 1$ at the receiver after the filtering step is carried out. As each data symbol is spread over N_c chips and further over N_d frames containing two pulses (a doublet) the signal energy can be expressed as $P_1 = 2N_d N_c \int [h^{(1)}(t)]^2 dt$, where $h^{(1)}(t)$ is the channel corresponding to the user of interest $i = 1$. $P_I = \sum_{i=2}^N P_i$ collects the energy P_i of all interfering sources $i = 2, \dots, N$. An example of a single user signal in the noiseless case, after propagation through the channel and subsequent filtering at the receiver is presented in figure 7. Further, in figure 6, a mixture of three users corresponding to $SIR = -10$ dB is depicted. Note that for both figures, the x-axis represents the number of samples, where sampling is performed at a rate of 10ps.

In figure 4, we present the recovery failure rate versus the signal to interference ratio. Any packet offset estimate $\hat{\tau}$ that does not fit into the range $\tau - T_c/2 < \hat{\tau} < \tau + T_c/2$ is considered to be a failure. The chosen interval is considered to provide sufficient recovery of the energy after

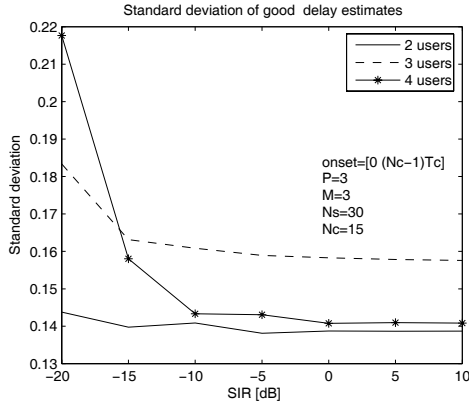


Figure 5. Std of the correctly estimated packet offset delays.

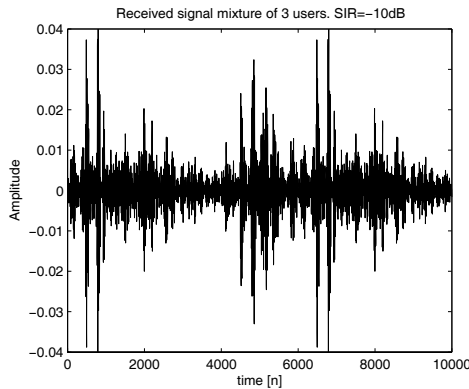


Figure 6. The mixture of three users at the receiver side for $SIR = -10\text{dB}$.

the deployment of a decorrelating receiver. Initially, we choose a TH and CDMA code. A Gold code sequence of length N_c is chosen for the latter one. Both codes remain unchanged in all Monte-Carlo runs. In each run, a new set of channels as well as packet offsets is assigned to each of the users and is kept the same for all the values of the SIR changed in steps of 5dB. $N_s = 30$ stands for the number of data symbols within a transmitted packet. The over-

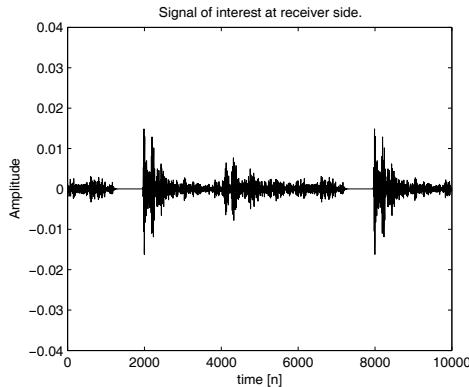


Figure 7. Sequence of doublets after the propagation through the channel(single user case).

sampling rate $P = 3$ equals the number of frames (doublets) per chip. Delays used in the time hopping scheme are chosen to be $D_1 = 1$ ns, $D_2 = 2$ ns, and $D_3 = 3$ ns. In figure 4, the solid, dashed and dash-asterisk line corresponds to the two, three and four user case, respectively. The performance of the algorithm drops by increasing the total number of users. This can be explained by an augmented influence of the cross-correlation terms as the number of users increases. However, in the four user case, the algorithm exhibits a low failure rate even in the event of $SIR = 0\text{dB}$, *i.e.*, in the case the signal of interest equals the energy of all interfering sources. This issue could be improved by a selection of user codes that would have low cross-correlation properties for any code offset.

Figure 5 describes the standard deviation of the estimates of τ , *i.e.*, $\hat{\tau}$. The y-axis depicts the deviation expressed as a fraction of the chip duration T_c . Due to the low number of Monte-Carlo iterations, and to the unresolvable ambiguity related to the initial sampling point, the '3 user' scenario has a slightly degraded performance compared to the other scenarios.

Acknowledgment

We would like to thank Zoubir Irahauten from Delft University of Technology for providing us the measured channel impulse responses.

References

- [1] L. Yang and G. Giannakis, "Ultra-wideband communications: an idea whose time has come," *Signal Processing Magazine, IEEE*, vol. 21, pp. 26–54, Nov. 2004.
- [2] D. Cassioli, M. Win, and A. Molisch, "The ultra-wide bandwidth indoor channel: From statistical model to simulations," *IEEE Journal on Selected Areas in Communications*, vol. 20, pp. 1247–1257, Aug. 2002.
- [3] R. Hocht and H. Tomlinson, "Delay-hopped transmitted-reference RF communications," in *IEEE Conference on Ultra Wideband Systems and Technologies*, pp. 265–270, 2002.
- [4] A. van der Veen, A. Trindade, Q. Dang, and G. Leus, "Signal model and receiver algorithms for a transmit-reference ultra-wideband communication system," *JSAC, Special issue on ultrawide band*, 2006.
- [5] R. Djapic, G. Leus, and A. J. van der Veen, "Blind synchronization in asynchronous UWB networks based on the transmit-reference scheme," in *Asilomar Conference on Signals, Systems, and Computers*, Nov. 2004.
- [6] R. Djapic, G. Leus, A. Trindade, and A. J. van der Veen, "Blind synchronization in multiuser transmit-reference UWB systems," in *Eusipco*, Sept. 2005.
- [7] M. Win and R. Scholtz, "Impulse radio: How it works," *IEEE Communications Letters*, Feb. 1998.
- [8] M. Torlak and G. Xu, "Blind multiuser channel estimation in asynchronous CDMA systems," *IEEE Trans. Signal Processing*, vol. 45, pp. 137–147, Jan. 1997.